coatings

MDPI

Article

Ca–Zn Phosphate Conversion Coatings Deposited on Ti6Al4V for Medical Applications

Diana-Petronela Burduhos-Nergis [1], Nicanor Cimpoesu [1], Elena-Luiza Epure [2], Bogdan Istrate [3], Dumitru-Doru Burduhos-Nergis [1] and Costica Bejinariu [1,*]

[1] Faculty of Materials Science and Engineering, Gheorghe Asachi Technical University, 700050 Iasi, Romania; nicanor.cimpoesu@academic.tuiasi.ro (N.C.)
[2] Department of Natural and Synthetic Polymers, Faculty of Chemical Engineering and Environmental Protection, "Gheorghe Asachi" Technical University of Iaşi, Str. Prof.dr.doc. D. Mangeron nr. 73, 700050 Iasi, Romania; lepure@tuiasi.ro
[3] Faculty of Mechanical Engineering, "Gheorghe Asachi" Technical University of Iasi-Romania, Blvd. Dimitrie Mangeron, No. 61–63, 700050 Iasi, Romania; bogdan.istrate@academic.tuiasi.ro
* Correspondence: costica.bejinariu@tuiasi.ro

Abstract: This paper aims to study the possibility of improving the chemical and surface characteristics of the Ti6Al4V alloy by depositing phosphate layers on its surface. Accordingly, an innovative phosphating solution was developed and used in a chemical conversion process to obtain Ca–Zn phosphate layers on the base material surface. Moreover, the chemical composition of the phosphate solution was chosen considering the biocompatibility of the chemical elements and their possibility of contributing to the formation of phosphate compounds. The obtained layer was characterized by optical microscopy (OM), scanning electron microscopy (SEM), energy dispersive spectroscopy (EDS), X-ray diffraction (XRD), Fourier-transform infrared spectroscopy (FTIR), and potentiodynamic polarization tests. The wetting of the Ca–Zn sample surface was also investigated using water and two liquids similar to body fluids, namely, Ringer and Dulbecco solutions. According to the surface energy study, the polar component is almost two times larger compared with the dispersive one. The SEM and EDS tests revealed a uniformly coated surface with intercalated crystals leading to a rough surface. Furthermore, the XRD results showed not only the presence of hopeite and scholzite but also of phosphophyllite. By the vibrations of the PO_4^{-3} groups, the FTIR test confirmed the presence of these phases. The potentiodynamic tests revealed that the samples coated with the Ca–Zn phosphate layer present better corrosion resistance and a lower corrosion rate compared with the uncoated ones.

Keywords: titanium alloy; phosphate layer; conversion coating; biomaterial; zinc phosphate; scholzite

Citation: Burduhos-Nergis, D.-P.; Cimpoesu, N.; Epure, E.-L.; Istrate, B.; Burduhos-Nergis, D.-D.; Bejinariu, C. Ca–Zn Phosphate Conversion Coatings Deposited on Ti6Al4V for Medical Applications. *Coatings* **2023**, *13*, 1029. https://doi.org/10.3390/coatings13061029

Academic Editor: Liqiang Wang

Received: 5 May 2023
Revised: 28 May 2023
Accepted: 29 May 2023
Published: 1 June 2023

1. Introduction

The number of people who need implants is increasing over time, either in response to trauma caused by accidents or degenerative bone diseases. Bone tissue engineering is concerned primarily with finding new biomaterials with superior properties or improving existing ones on the market [1]. Titanium is one of the most popular materials used in the medical field; it is found in hip prostheses, knee prostheses, dental implants, etc. This is due to the fact that, in addition to being biocompatible, it has superior mechanical properties as well as acceptable corrosion resistance [2,3].

However, there is a risk of implant rejection or failure due to titanium's bioinert surface [4]. Therefore, over time, different methods have been tried to promote the osteogenic activity and stability of titanium (or titanium alloy) implants. These methods include mechanical processing [5–7] (grinding, polishing, sandblasting, laser cavitation, etc.) and acidic treatments [8,9] that are conducted to obtain a surface with high roughness. The surface roughness is important to promote tissue regeneration and the anchoring of further deposited layers. Several studies were also investigated the protection of Ti implants

against corrosion by coating their surfaces with different types of thin layers. For example, many researchers have been studying the deposition of hydroxyapatite on the Ti surface since the 1980s until now [10,11]. Hydroxyapatite layers can be deposited by different methods, including micro-arc oxidation [12], the sol–gel method [13], the plasma spraying method [14], electrodeposition [15], the ion-beam deposition method, etc. [16–18]. Other researchers have deposited nitride layers, such as zirconium nitride, titanium nitride, etc., using different methods such as the Physical Vapor Deposition method (PVD) [19–21]. Using the same techniques as previously mentioned, the osseointegration of titanium can also be promoted by coating its surface with different types of oxides, such as CuO, ZnO, ZrO_2, etc. [22]. Considering the advantages related to their ease of use, electrodeposition and PVD are two of the most used methods to cover a Ti surface.

Due to the importance of human health and the high use of titanium implants, it is still of great interest to find new solutions or to improve existing ones that contribute to Ti implant acceptance and biointegration. Accordingly, in recent years, numerous studies have focused on the improvement of titanium alloy characteristics by depositing different types of phosphate layers. Due to its multiple advantages, this chemical conversion process has garnered great interest from different industries (automotive, construction sector, etc.), but its suitability for bioengineering was only discovered recently [23]. Some of the strong points of this process are its low economic cost, high adherence to the substrate, and, of course, the high corrosion resistance of the resultant coating [24,25]. Considering the versatility of the phosphate solutions (they can incorporate different types of metals), biocompatible elements that can promote the osseointegration of the substrate can be deposited onto its surface while also protecting the base materials against corrosion [26,27]. The characteristics of the phosphate layer and its anchorage to the substrate surface are strongly influenced by multiple factors. Liu et al. [28] studied the influence of the pH of the phosphate solution on the structure of the Ca–Zn phosphate layer deposited on pure titanium. According to their publication, both hopeite and scholzite phases can be deposited on the substrate surface. Hopeite is created in higher amounts at pHs between 2.50–3.25, while higher quantities of the scholzite phase can be observed at pHs between 3.50–4.25. In this case, corrosion tests revealed that the samples with a higher content of hopeite had superior corrosion resistance to those where scholzite was predominant. The same group of researchers also published another study regarding the influence of temperature on the crystals' structure [29]. In their publication, they observed that by increasing the immersion time and temperature, the coating structure (compactness) and thickness could be improved. Zhao et al. [30] studied the effect of voltage and temperature on the formation of Ca–Zn phosphate layers. Compared with the previously cited studies, in this research, the coating was obtained through an electrolysis-induced phosphate chemical conversion method. Accordingly, the authors observed that the corrosion resistance and the structural characteristics of the deposited layer can be improved if the voltage is decreased and the temperature is increased. Liu et al. [31] also studied the biocompatibility of scholzite coatings deposited on the surfaces of pure Ti and Ti6Al4V, demonstrating that this type of process and coating can be used in order to promote the osteointegration of titanium and its alloys.

According to the reviewed studies, the deposition of phosphate layers by chemical conversion is a suitable method for promoting the biointegration of Ti implants; however, there are very few studies that consider Ti6Al4V as a substrate, and many of the parameters that influence layer formation were not considered. Furthermore, the literature is very poor in terms of the types of phosphating solutions that can be used to obtain protective layers for Ti implants. In this study, an innovative phosphating solution was developed, which was further used in a chemical conversion process to obtain Ca–Zn phosphate layers on the Ti6Al4V surface. Moreover, the chemical composition of the phosphate solution was chosen considering the biocompatibility of the chemical elements and their possibility of contributing to the formation of phosphate compounds. Accordingly, a new phase was confirmed in the structure of the deposited layer, while relevant tests were employed to

analyze the layer morphology and its corrosion resistance in two types of corrosive media (Ringer and Dulbecco solutions) relevant for bioengineering applications.

2. Materials and Methods

2.1. Materials

Due to their biocompatibility and good mechanical properties, titanium alloys are widely used for implant manufacturing. In this study, Ti6Al4V purchased from AEMMetal (Hunan, China) was used as a substrate. The material was supplied in a round bar form, and its chemical composition, provided by the supplier, is presented in Table 1.

Table 1. Chemical composition of Ti6AL4V used as substrate.

Element	Al	V	Fe	O	C	Ti
wt.%	6.14	4.22	0.12	0.11	0.028	bal.

2.2. Sample Preparation

The Ti6Al4V bars were cut into specimens with a size of Ø10 mm and a thickness of 3 mm. In order to promote the biointegration of the titanium alloy, a phosphate layer was deposited onto the surface of the obtained samples by a chemical conversion process (phosphating). First, the samples were ground with 400, 600, 800, 1000, and 1200 grit SiC abrasive paper. After a homogenous surface was obtained, the samples were degreased by immersing them successively in an ultrasonic bath with acetone, ethyl alcohol, and distilled water for 10 min. Following that, the surface was pickled and activated by immersing the samples in a 2% HF solution for 15 s, followed by 30 s in a 3 g/L titanium colloidal solution ($Na_4TiO\ (PO)_2\ 0–7H_2O$). Then, a Ca–Zn phosphate layer was deposited on the samples surfaces by immersing them in a phosphating solution. The phosphating step took place for 60 min at 90 °C. The chemical composition of the phosphating solution used in this research is different from the ones previously presented in the literature. The solution used here contains the following accelerators and inhibitors: HNO_3, NaOH, $NaNO_2$, $Na_5P_3O_{10}$, and NaF in different quantities—the influence of each component was described in Ref. [32]. In addition, in this solution, $Ca(NO_3)_2$, Zn chips, Fe powder, and H_3PO_4 were added to obtain the metal cations and compounds that will conduct to the phosphate layer formations. Afterwards, the samples were rinsed in cold water and dried at room temperature. A schematic representation of the phosphating process is presented in Figure 1.

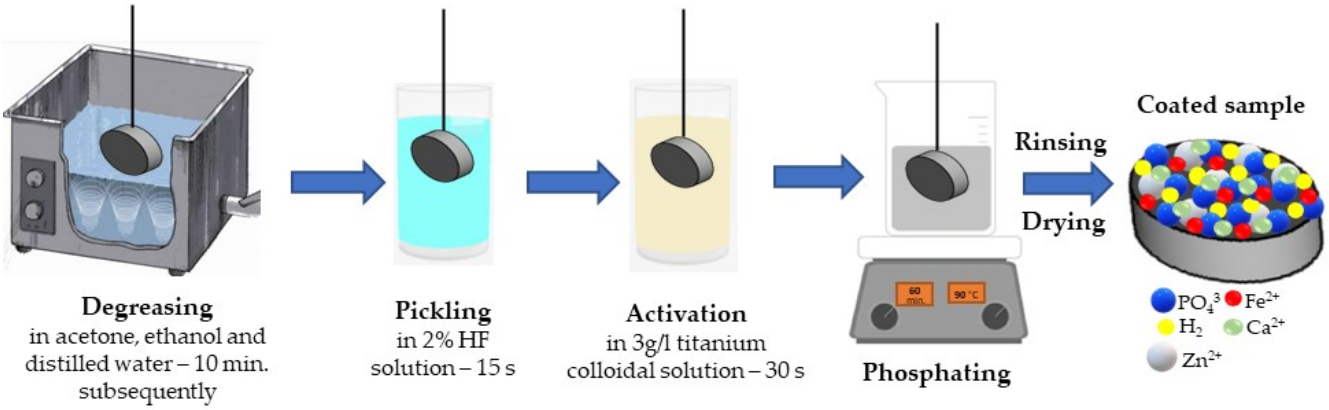

Figure 1. The process flow chart of sample coating.

2.3. Methods

The morphology and the chemical composition of the deposited layer were studied using an optical microscope (Zeiss Imager Axio a1M) and a scanning electron microscope (Vega Tescan LMH II) equipped with an energy dispersive detector (EDAX Bruker). The

chemical composition of the layer was determined by making 5 measurements at different points of the surface of the samples; in this study, the measurement closest to the average is presented.

The type of crystals which were formed on the surface of the titanium alloy Ti6Al4V was determined using an X-ray diffractometer (PANalytical X'Pert PRO MPDR) using Cu-Kα1 radiation. This study used a 2θ angle ranging between 5°–70°, the number of steps was 6474, and the step size was 0.0131° every 60 s with a scanning speed of 0.054 °/s. In order to highlight the compounds specific to the obtained phosphate layer, a Fourier-transform infrared spectroscope (Bruker Hyperion 1000 FTIR spectrometer) was used with a wavenumber range between 4000 cm^{-1} and 600 cm^{-1} at a spectral resolution of 4 cm^{-1} and several 64 scans for each analyzed surface.

Because this material was designed to be used as an implant, an indispensable property is the hydrophilic surface. To determine this kind of characteristic, the contact angle was evaluated. For this determination, a Drop Shape Analyzer (DSA100, Kruss) with a software-controlled dosing system was used, and the contact angle was measured through the sessile-drop method. The wettability of the metal surface was tested by deionized water, ethylene glycol, and Ringer and Dulbecco solutions at room temperature. The volume of the drop deposited on the metal piece was 4 µL. After the drop was deposited, the contact angle was recorded for 60 s. The metal surface was cleaned with high-purity ethanol and dried before the contact angle tests. For each liquid sample, measurements were carried out at least five times. The average of all the individual measurements was used to compute the contact angle value [33]. Additionally, the Owens–Wendt–Rabel–Kaelble (OWRK) method [34] based on contact angle was used to calculate the sample's surface energy.

The corrosion properties of the Ca–Zn phosphate layer were analyzed by potentiodynamic polarization in two different corrosion media. In this study, Ringer solution (pH = 6.18) and Dulbecco's phosphate-buffered saline solution without Ca and Mg (pH = 7.4) were used to evaluate the corrosion resistance of the obtained samples. The potentiodynamic polarization tests were conducted using an OrigaFlex potentiostat equipped with a three-electrode cell. The cell includes a reference electrode (saturated calomel electrode), a platinum counter electrode, and the working electrode (the analyzed sample). The analyzed sample has an exposed area of 0.785 cm^2. The obtained results were processed with OrigaMaster 5 software (Version 2.5.0.3.). The polarization curves were obtained at a potential range of (−300) to (+300) mV vs. o . . . pen circuit potential (OCP), with a scan rate of 0.5 mV/s. The electrochemical tests were repeated 3 times to ensure their repeatability.

3. Results and Discussion

3.1. Characterization of the Ca–Zn Phosphate Layer

Optical and scanning electron microscopy were used to study the structure and the uniformity of the coating. Figure 2 presents the images obtained by OM at a magnification of 5×, 10×, and 20×, while Figure 3 shows the SEM micrographs for the Ca–Zn phosphate layer deposited on the Ti6Al4V surface.

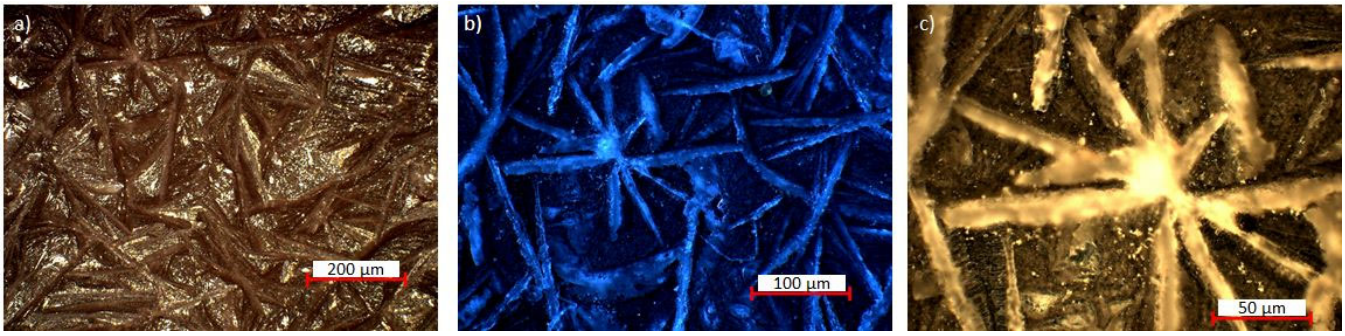

Figure 2. Optical microstructure of the Ca–Zn phosphate layer deposited on the Ti6Al4V surface viewed at (**a**) 5×, (**b**) 10×, and (**c**) 20× magnification.

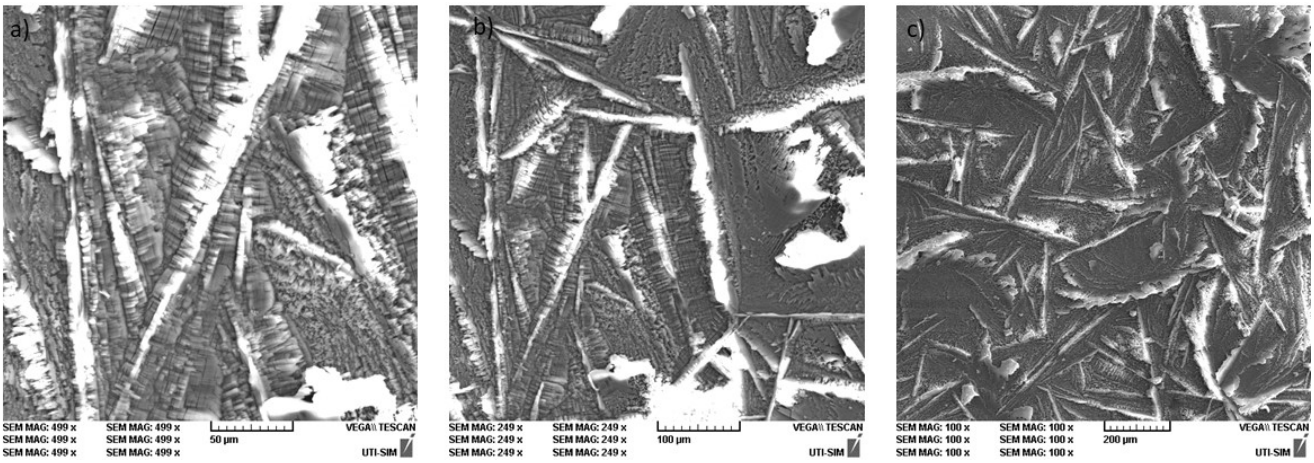

Figure 3. The morphology of the Ca–Zn phosphate layer deposited on the Ti6Al4V surface viewed at (**a**) 500×, (**b**) 250× and (**c**) 100× magnification.

A morphology specific to many crystals of different sizes can be observed uniformly deposited all over the surface of the titanium alloy (Figure 3c). Due to the areas between the crystals, called inter-crystalline areas, the surface of the layer is rough, which is specific to phosphate layers deposited by the chemical conversion process. The average roughness value (Ra) of the obtained coatings, determined by profilometry, was around 1.34 µm. This aspect represents an advantage of these layers since they can facilitate cell adhesion, similarly to the porous structure of bones. The formed crystals are compact, having an acicular shape in some areas (Figure 3b) and a flower shape in others (Figure 2b,c). The flower-like structure is specific to the hopeite compound created after phosphating, and its presence was confirmed by XRD analysis. Compared with other phosphate layers based on Zn and Ca, the morphology of those obtained in this study is different from that obtained by Liu et al. [31]. In their study, the authors observed that the crystals they obtained have the typical morphology of scholzite, being composed of smaller and thicker lamellar crystals. Another study [29] shows that the structure of crystals obtained on a pure Ti surface looks like flakes, with their dimensions depending on the temperature (25 °C, 55 °C, 75 °C) of the phosphate solution. Therefore, the structure of the Ca–Zn phosphate layer differs depending on the process parameters (immersion time, phosphating temperature, coupled systems, coupling voltage, sample preparation process, etc.) and very much on the chemical composition of the phosphating solution. In this case, the crystal's dimensions could be higher than those presented previously due to the high phosphating temperature (90 °C).

In order to observe the uniformity of the chemical composition of the deposited layer, the sample surface was analyzed by EDS and examined from five different points of view from the chemical composition point of view. Figure 4 shows the chemical element distribution in the area of the Ca–Zn phosphate layer, where the chemical composition is close to the average of the five different points. In addition, the chemical composition and the energy spectra of this zone are presented in Figure 5. The SEM and EDS analyses were also used to evaluate the thickness of the obtained phosphate layer. Figure 6 shows the morphology of the coated samples in cross-section; the average thickness layer is around 63 µm.

As can be seen from Figure 4, the elemental distribution confirms the presence of P, O, Zn, Ca, and Fe all over the analyzed surface. The presence of Ti, V, and Al is explained by the penetration of X-rays up to the interface between the phosphate layer and the titanium alloy substrate in those areas where the phosphate layer is thinner. This aspect was also observed by other researchers looking at phosphate conversion coatings deposited on titanium or other alloys [30,32].

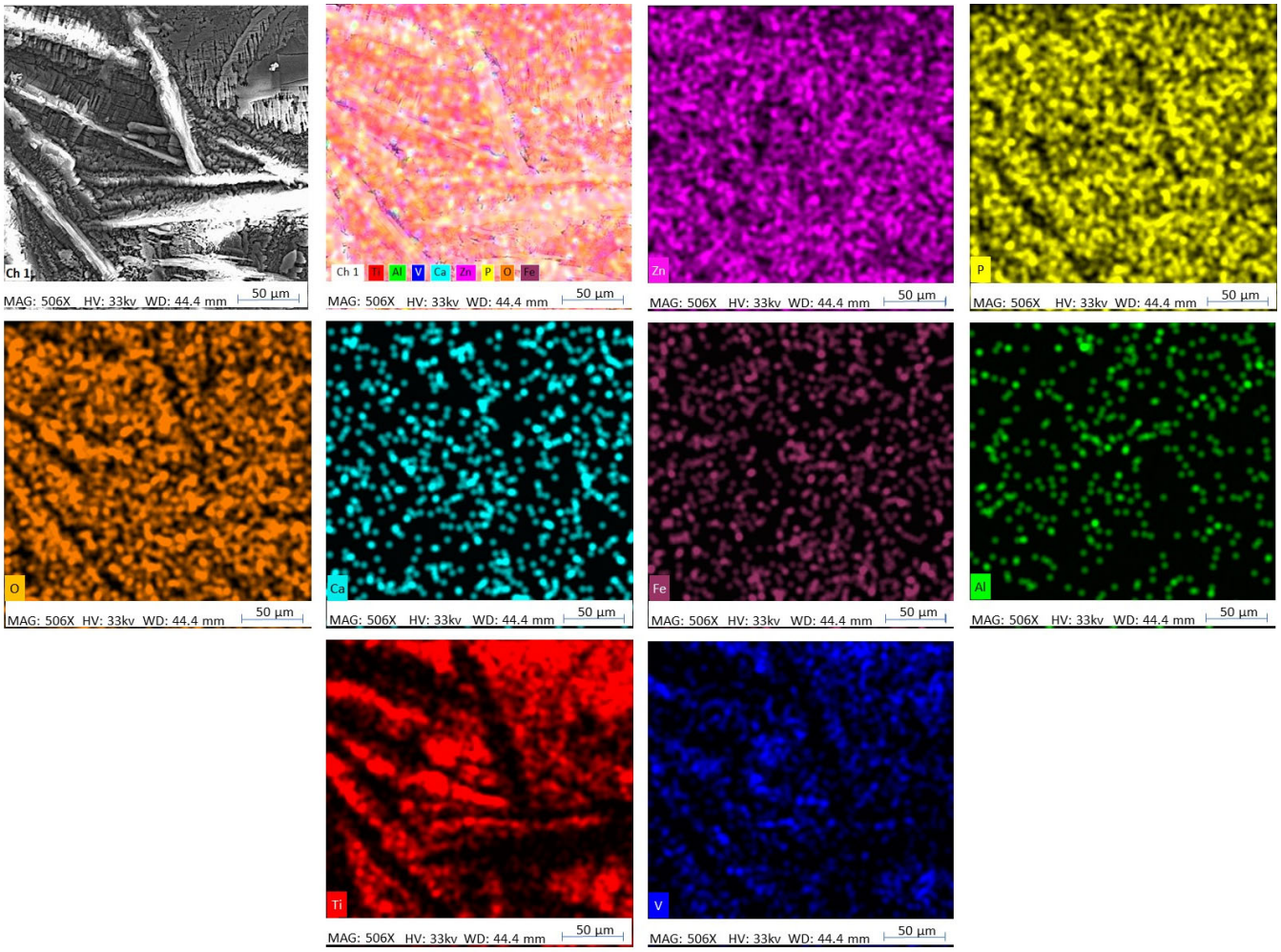

Figure 4. EDS area scan of the Ca–Zn phosphate layer.

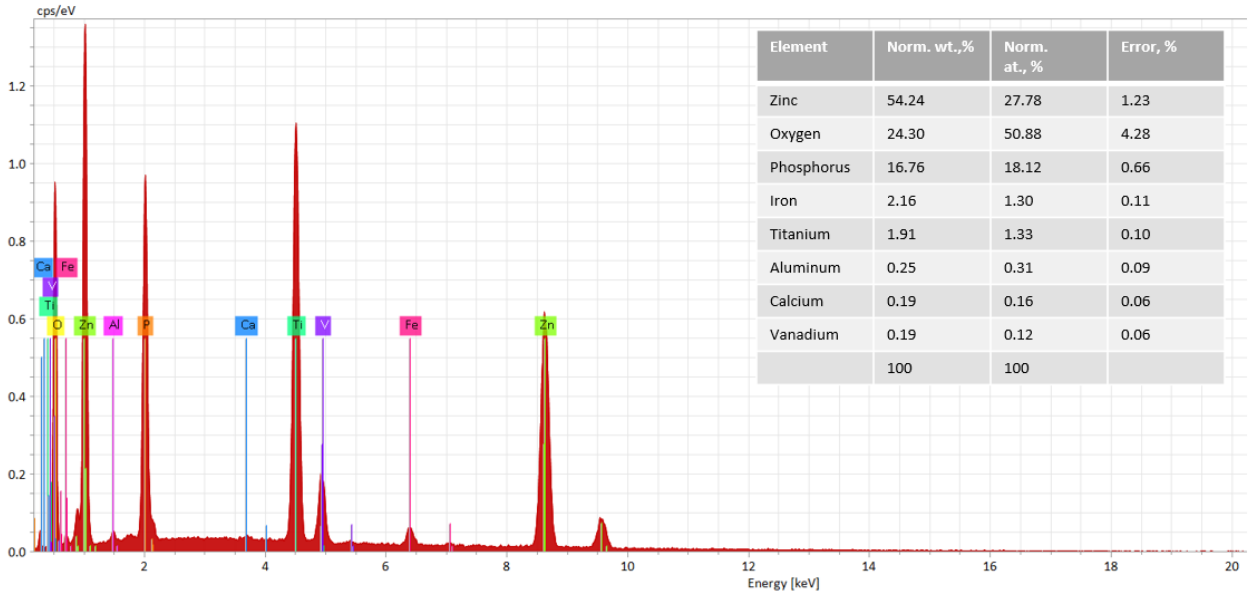

Element	Norm. wt.,%	Norm. at., %	Error, %
Zinc	54.24	27.78	1.23
Oxygen	24.30	50.88	4.28
Phosphorus	16.76	18.12	0.66
Iron	2.16	1.30	0.11
Titanium	1.91	1.33	0.10
Aluminum	0.25	0.31	0.09
Calcium	0.19	0.16	0.06
Vanadium	0.19	0.12	0.06
	100	100	

Figure 5. Energy spectra and the chemical composition of the Ca–Zn phosphate layer.

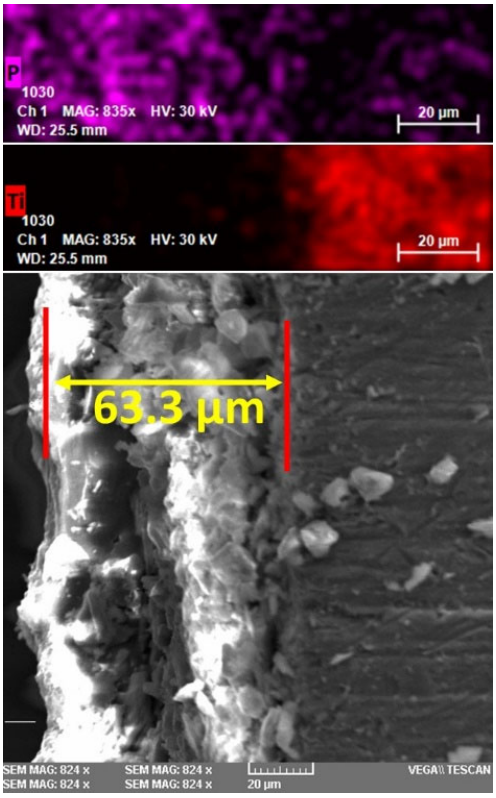

Figure 6. SEM–EDS image of the cross-section of the coated sample.

In order to determine the phase formed on the surface of the Ti6Al4V by depositing a Ca–Zn phosphate layer through the chemical conversion process, an XRD analysis was conducted. The XRD diffractogram of the coated sample is presented in Figure 7.

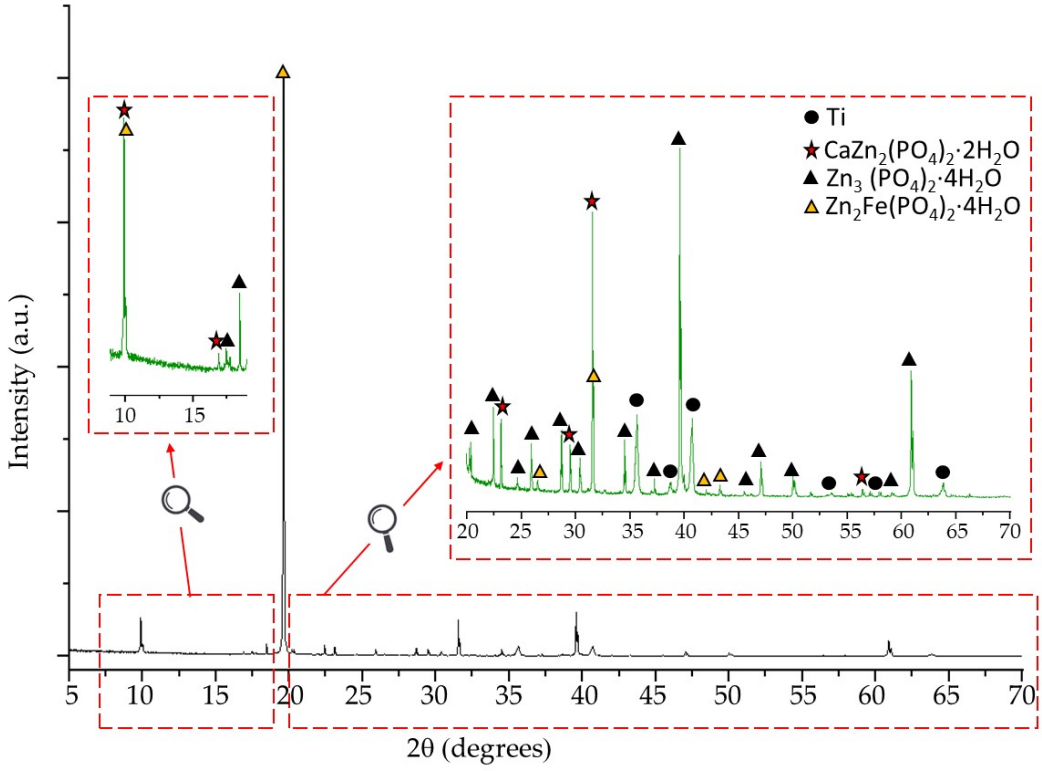

Figure 7. XRD diffractogram of the Ca–Zn phosphate layer.

The XRD pattern presents significant peaks of specific phases which can be indexed as scholzite ($CaZn_2(PO_4)_2 \cdot 2H_2O$, PDF 04-010-2736), hopeite ($Zn_3(PO_4)_2 \cdot 4H_2O$, PDF 04-015-0707), and phosphophyllite ($Zn_2Fe(PO_4)_2 \cdot 4H_2O$, PDF 01-074-6617 and PDF 04-011-6924).

As can be observed, the strongest diffraction intensity is specific to the phosphophyllite phase at a 2θ degree of 19.7° corresponding to the (002) crystal plane. Furthermore, the $Zn_2Fe(PO_4)_2 \cdot 4H_2O$ phase is detected at 2θ degree of 9.9°, 26.4°, 31.5°, 41.2°, 43.4° corresponding to the (100), (112), ($\bar{3}$12), (400), and ($\bar{4}$14) crystal planes. Regarding the zinc phosphate tetrahydrate compound, hopeite shows many significant peaks, including one with high intensity at a 2θ degree of 39.6° corresponding to the (080) crystal plane. Due to the introduction of Ca in the phosphate solution, another phase formed is scholzite, which has two peaks with remarkable intensity at a 2θ degree of 10.1° and 31.7° corresponding to the (200) and (1422) crystal planes, respectively. According to the XRD analysis, the highest number of peaks is specific to hopeite. Thus, the addition of Ca and Fe in the phosphate solution formed specific compounds which will improve the characteristics of the TI6Al4V substrate.

An FTIR spectrum of the Ca–Zn phosphate layer is shown in Figure 8. As can be seen, the vibration band between 600–700 cm^{-1} has a significant peak at 607 cm^{-1}; this band can be assigned to the stretching vibration of hydroxyl groups or PO_4^{-3} groups [35]. The O-H group can appear due to the motion of the absorbed water [36]. In addition, significant peaks are presented between 3100–3600 cm^{-1}, which can also be attributed to O-H groups that can indicate the existence of crystal water [30]. This aspect is available also for the peak between 1500–1700 cm^{-1}. The peak at 1041 cm^{-1} can be attributed to the PO_4^{-3} group, which is part of all the identified phases from the XRD results. Furthermore, the peak at 964 cm^{-1} and the vibration band between 900–1200 cm^{-1} correspond to the P-O stretching in HPO_4^2 [37].

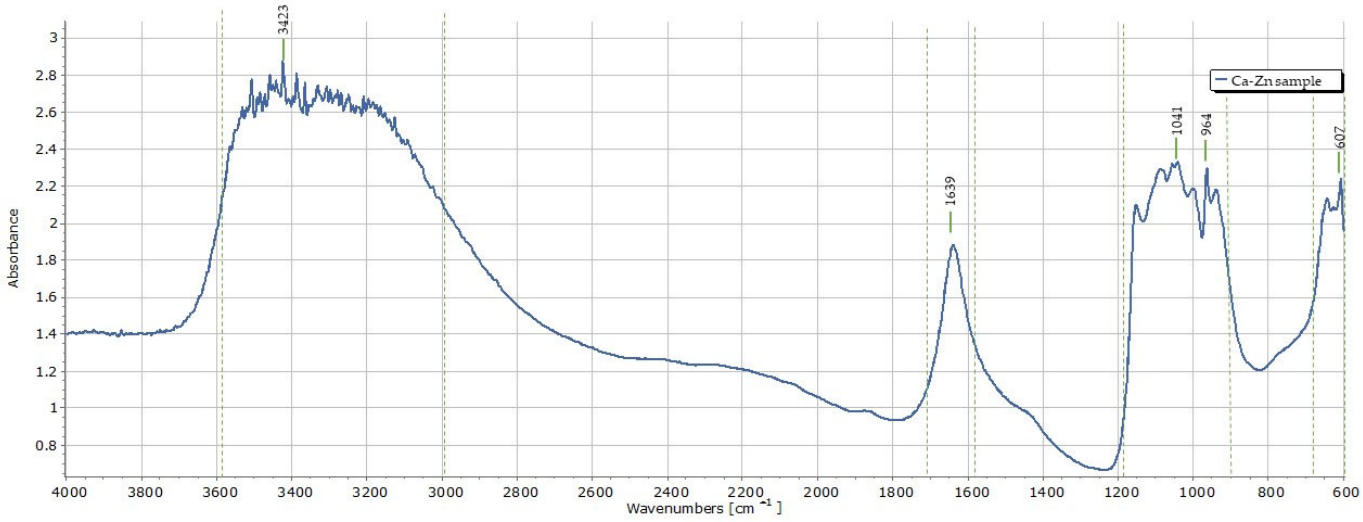

Figure 8. FTIR spectra of the Ca–Zn phosphate layer.

3.2. Corrosion Characteristics

Figure 9 shows the potentiodynamic polarization curves of Ti6Al4V coated with a Ca–Zn phosphate layer (Ca–Zn) and Ti6Al4V uncoated samples, tested in Dulbecco solution (Figure 9a) or Ringer solution (Figure 9b). The corrosion parameters of E_{corr}, I_{corr}, β_a, β_c, polarization resistance (R_p) and corrosion rate (C_R) were calculated with formulas presented in a previous study [25] and are summarized in Table 2. In both cases, Ti6Al4V specimens were tested as control samples in order to reveal the influence of the coating on the corrosion properties of the titanium alloy.

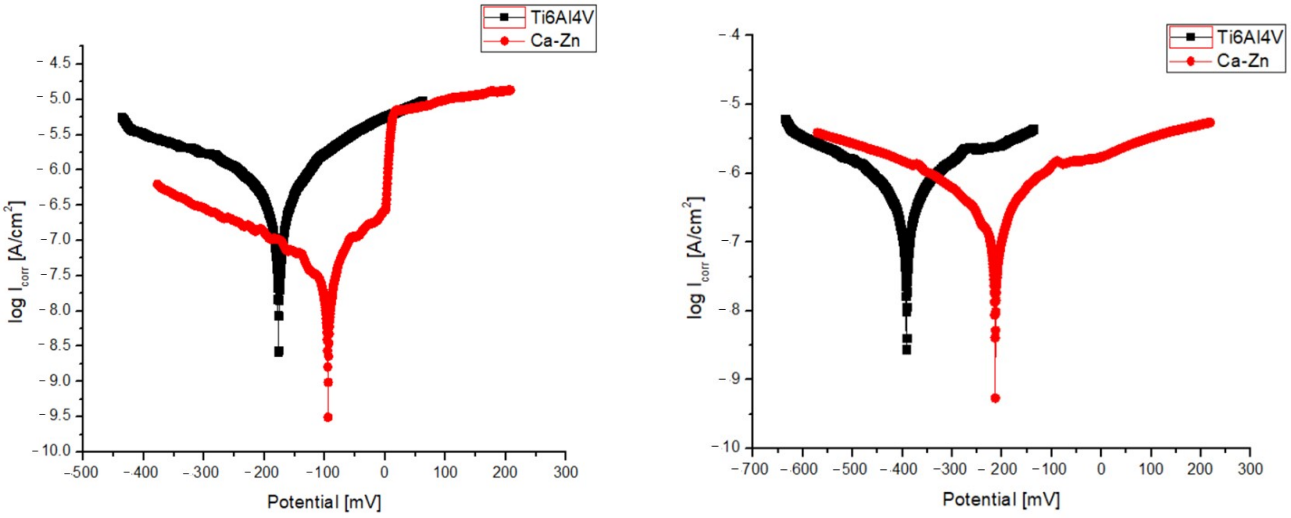

Figure 9. Potentiodynamic polarization curves of uncoated Ti6Al4V or Ti6Al4V coated with a Ca–Zn phosphate layer tested in Dulbecco solution (**a**) or Ringer solution (**b**).

Table 2. Electrochemical corrosion parameters determined for the Ca–Zn phosphate layer and uncoated Ti6Al4V tested in the two corrosive media.

Sample	Corrosive Media	E_{corr} mV	I_{corr} μA/cm^2	β_a mV/dec.	β_c mV/dec.	R_p kΩ·cm^2	C_R μm/Year
Ti6Al4V	Dulbecco	−177	0.63	172	−270	87.8	13.15
Ca–Zn		−95	0.02	53	−131	419.5	0.46
Ti6Al4V	Ringer	−448	0.86	100	−106	17.9	18.03
Ca–Zn		−213	0.04	38	−59	101.1	0.95

As can be seen from Figure 9, the anodic curve specific to the Ca–Zn sample presents a slope change near 0 mV, indicating the start of a passivation plateau within the increase of potential. Moreover, for both cases, the curves of the phosphate sample shifted to a positive direction of corrosion potential while current density decreased significantly compared with the values of the uncoated Ti6Al4V samples. These results show that the phosphate samples present a higher corrosion resistance due to the small values of I_{corr} (0.02 and 0.04 μA/cm^2) and more positive values of E_{corr} (−95 and −213 mV) compared with the high values of I_{corr} (0.63 and 0.86 μA/cm^2) and more negative values of E_{corr} (−177 and −448 mV) for uncoated samples. It is also well known that a high value of polarization resistance indicates a good corrosion resistance; therefore, the values of R_p for the Ca–Zn sample are about five times higher compared with Ti6Al4V samples. At the same time, the corrosion rate decreased significantly from 13.15 and 18.03 μm/year for uncoated samples to 0.46 and 0.95 μm/year for the coated ones. Furthermore, regardless of the sample type (coated or uncoated), the results show that the Ringer solution is more corrosive compared with the Dulbecco solution.

Another study [31] regarding the deposition of scholzite and hopeite on the surface of titanium by phosphating revealed an improvement of corrosion resistance in 0.9% NaCl solution. As in this research, the corrosion potential for the coated samples exhibited more positive values (from −440 mV to −310 mV) and lower current density values (from 0.53 to 0.37). Compared with the results of our study, even though the corrosive media are different, we can observe an improvement of corrosion resistance due to the presence of the phosphophyllite phase.

3.3. Surface Wettability

The contact angle values can be influenced by surface texture, chemistry, and cleanliness. Other variables that affect the contact angle measurement include the experimental temperature, the volume, and the kind of liquid employed. The contact angle was tested for water, ethylene glycol, and Ringer and Dulbecco solutions at room temperature. The measurements were carried out for 60 s following/after the drop's deposition. For all liquids, it was found that the contact angle dramatically decreases in the first 10 s, then stabilizes in the next 20–60 s, reaching a plateau value. The decreasing contact angle values could be explained by a very low spreading of the drop until this reaches thermodynamic equilibrium. In this case, the droplet spreading occurs on a fast-time scale with minimal fluid penetration into the surface layer, the surface being porous as revealed by SEM. After the spreading phase is through, the volume loss from the droplet to the substrate occurs on a slow-time scale [38]. The average of all measurements for each liquid sample is shown in Table 3, along with its standard deviation.

Table 3. Contact angle values of the liquids deposited on the Ca–Zn sample.

No.	Solution	Contact Angle (°)
1	Water	58.3 ± 2.1
2	Ringer solution	56.0 ± 5.2
3	Dulbecco solution	68.5 ± 5.2
4	Ethylene glycol	34.5 ± 3.2

Images of the water, Ringer, and Dulbecco solution droplets deposited on the metal surface are shown in Figure 10.

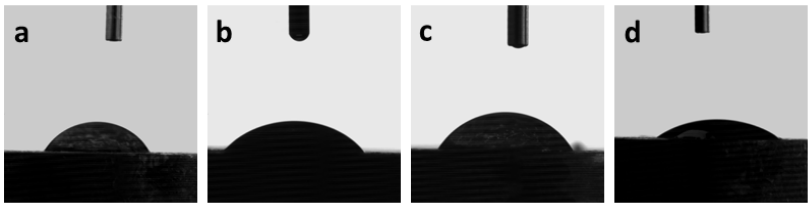

Figure 10. The sessile drop of water (**a**), Ringer solution (**b**), Dulbecco solution (**c**) and ethylene glycol (**d**).

All testing solutions, having a contact angle less than 90°, wet the Ca–Zn coated sample (Table 3). Comparing the liquids related to the body fluids, the capacity to wet the metal surface is almost the same for the water and Ringer solution, with a slightly better value for the latter one. Amongst the three body fluids, the Dulbecco solution has the lowest surface-wetting capacity, presenting the highest contact angle value. Because of its lower contact angle, the Ringer solution is more attracted to and retained on the sample's surface. The coating appears to have grown permeable over time, enabling liquid to pass through it and moisture to reach the underlying material and start corrosion processes. The test corrosion revealed that the Ringer solution is more corrosive than the Dulbecco solution, which has a bigger contact angle than the Ringer solution. An inverse correlation between contact angle values and corrosion rates was reported for super-hydrophobic surfaces [39], but with a different explanation for this phenomenon. The metal surface is hydrophilic, as evidenced by the contact angle between the water and the sample, which is 58.3 ± 2.1°.

The spread of the liquid drops over the metal surface is due to cohesive (the magnitude of the interactions among a material's molecules) and adhesive forces (intensity of the interactions with molecules from other materials) that develop on the liquid's molecules. In this regard, surface energy is a reliable indicator of the degree of wettability [34]. Based on contact-angle values, the sample's surface energy was calculated using the Owens–Wendt–Rabel–Kaelble (OWRK) method [34], based on Fowkes' theory. According to this

theory, the surface energy is the sum of dispersion, polar, hydrogen, induction, and acid-base interactions. In the OWRK methods, the interactions were divided into two types: dispersive (van der Waals) and polar (Equation (1)).

$$\gamma_s = \gamma_s^d + \gamma_s^p \quad (1)$$

where γ_s^d and γ_s^p are the dispersive and polar components of the surface energy of the solid, respectively.

At least two test liquids with well-known polar and dispersive interactions are necessary for the OWRK model (Equation (2)) [40]. Thus, two liquids with different polarities were used to determine the surface energy of the metallic sample: water (polar solvent) and ethylene glycol (partially polar solvent).

$$\sqrt{\gamma_s^d \gamma_l^d} + \sqrt{\gamma_s^p \gamma_l^p} = 0.5[\gamma_l(1 + cos\theta)] \quad (2)$$

where γ_s^d, γ_s^p are dispersive components and γ_l^d, γ_l^p are polar components of the solid and liquid surface energies, respectively; γ_l is the surface tension of the liquid; and θ is the contact angle.

It was calculated that the total surface energy (γ_s) of the coated sample is 42.49 (±1.64) (mN/m). The polar and dispersive components of the total surface tension of the solid are as follows: γ_s^p= 27.57 (±0.79) (mN/m) and γ_s^d = 14.92 (±0.85) (mN/m). The higher polar component of the surface energy is due to the Ca–Zn phosphate layer, which was also highlighted by the XRD and FTIR studies. The long-range London dispersion forces are responsible for the dispersive forces. The significant part of the polar component can explain the affinity of the metal sample for polar liquids.

4. Conclusions

In this study, a new phosphating solution for obtaining a Ca–Zn phosphate layer on the Ti6Al4V surface was developed. In addition, relevant analyses were conducted to validate the formation of the coating layer and its potential improvements in the corrosion resistance of the base material.

A Ca–Zn phosphate layer was deposited on the surface of Ti6Al4V in order to study the possibility of improving the osteointegration of implants by increasing the corrosion resistance and the surface roughness. The SEM micrographs revealed that the deposited layer has a crystalline structure, specific to the zinc phosphate layer, where crystals are intercalated. The EDX, XRD, and FTIR analyses showed that hopeite, phosphophyllite, and scholzite crystals were formed all over the titanium alloy surface.

Both the coated and the base materials have been tested in two corrosion media (Ringer and Dulbecco solutions). The electrochemical tests revealed that the Ti6Al4V corrosion resistance was highly improved by depositing a Ca–Zn phosphate layer onto its surface, and the polarization resistance significantly increased by almost five times for the coated samples in both corrosion media. Moreover, the experiments revealed that the Ringer solution is a more aggressive corrosion media than the Dulbecco solution.

All solutions considered show satisfactory surface wettability. The wettability gradually increased from the Ringer solution to water and finally to the Dulbecco solution. From surface energy calculations, it was found that the coated Ti6Al4V has a predominantly polar surface, with the polar component being almost two times larger compared with the dispersive one. This polarity of the surface created by phosphating can be suitable for cell adhesion; therefore, future studies should be conducted on this topic.

Author Contributions: Conceptualization, writing, and investigation: D.-P.B.-N.; writing the original draft, project administration, and scientific supervision: D.-P.B.-N. and C.B.; methodology, investigation, data curation, and validation: E.-L.E., N.C., B.I. and D.-D.B.-N.; data curation, validation, and writing—reviewing and editing: D.-P.B.-N. and D.-D.B.-N.; resources and formal analysis: C.B. All authors have read and agreed to the published version of the manuscript.

Funding: This research received no external funding.

Institutional Review Board Statement: Not applicable.

Informed Consent Statement: Not applicable.

Data Availability Statement: Not applicable.

Acknowledgments: This paper was realized with the support of COMPETE 2.0 project nr.27PFE/2021, financed by the Romanian Government, Minister of Research, Innovation and Digitalization. This paper was also supported by "Gheorghe Asachi" Technical University from Iaşi (TUIASI), through the Project "Performance and Excellence in postdoctoral research 2022".

Conflicts of Interest: The authors declare no conflict of interest.

References

1. Bandyopadhyay, A.; Mitra, I.; Goodman, S.B.; Kumar, M.; Bose, S. Improving Biocompatibility for next Generation of Metallic Implants. *Prog. Mater. Sci.* **2023**, *133*, 101053. [CrossRef] [PubMed]
2. de Viteri, V.S.; Fuentes, E.; de Viteri, V.S.; Fuentes, E. Titanium and Titanium Alloys as Biomaterials. *Tribol.—Fundam. Adv.* **2013**, *1*, 154–181. [CrossRef]
3. Sidambe, A.T. Biocompatibility of Advanced Manufactured Titanium Implants—A Review. *Materials* **2014**, *7*, 8168. [CrossRef] [PubMed]
4. Silva, R.C.S.; Agrelli, A.; Andrade, A.N.; Mendes-Marques, C.L.; Arruda, I.R.S.; Santos, L.R.L.; Vasconcelos, N.F.; Machado, G. Titanium Dental Implants: An Overview of Applied Nanobiotechnology to Improve Biocompatibility and Prevent Infections. *Materials* **2022**, *15*, 3150. [CrossRef] [PubMed]
5. Kuji, C.; Soyama, H. Mechanical Surface Treatment of Titanium Alloy Ti6Al4V Manufactured by Direct Metal Laser Sintering Using Laser Cavitation. *Metals* **2023**, *13*, 181. [CrossRef]
6. Tsuji, A.; Jia, P.; Takizawa, M.; Murata, J. Improvement in the Polishing Characteristics of Titanium-Based Materials Using Electrochemical Mechanical Polishing. *Surf. Interfaces* **2022**, *35*, 102490. [CrossRef]
7. Xue, T.; Attarilar, S.; Liu, S.; Liu, J.; Song, X.; Li, L.; Zhao, B.; Tang, Y. Surface Modification Techniques of Titanium and Its Alloys to Functionally Optimize Their Biomedical Properties: Thematic Review. *Front. Bioeng. Biotechnol.* **2020**, *8*, 1261. [CrossRef]
8. Jemat, A.; Ghazali, M.J.; Razali, M.; Otsuka, Y. Surface Modifications and Their Effects on Titanium Dental Implants. *Biomed. Res. Int.* **2015**, *2015*, 791725. [CrossRef]
9. Doe, Y.; Ida, H.; Seiryu, M.; Deguchi, T.; Takeshita, N.; Sasaki, S.; Sasaki, S.; Irie, D.; Tsuru, K.; Ishikawa, K.; et al. Titanium Surface Treatment by Calcium Modification with Acid-Etching Promotes Osteogenic Activity and Stability of Dental Implants. *Materialia* **2020**, *12*, 100801. [CrossRef]
10. Albrektsson, T.; Lekholm, U. Osseointegration: Current State of the Art. *Dent. Clin. N. Am.* **1989**, *33*, 537–554. [CrossRef]
11. Satomi, K.; Akagawa, Y.; Nikai, H.; Tsuru, H. Tissue Response to Implanted Ceramic-Coated Titanium Alloys in Rats. *J. Oral. Rehabil.* **1988**, *15*, 339–345. [CrossRef] [PubMed]
12. Wang, Y.; Yu, H.; Chen, C.; Zhao, Z. Review of the Biocompatibility of Micro-Arc Oxidation Coated Titanium Alloys. *Mater. Des.* **2015**, *85*, 640–652. [CrossRef]
13. Jaafar, A.; Schimpf, C.; Mandel, M.; Hecker, C.; Rafaja, D.; Krüger, L.; Arki, P.; Joseph, Y. Sol–Gel Derived Hydroxyapatite Coating on Titanium Implants: Optimization of Sol–Gel Process and Engineering the Interface. *J. Mater. Res.* **2022**, *37*, 2558–2570. [CrossRef]
14. Kuo, T.Y.; Chin, W.H.; Chien, C.S.; Hsieh, Y.H. Mechanical and Biological Properties of Graded Porous Tantalum Coatings Deposited on Titanium Alloy Implants by Vacuum Plasma Spraying. *Surf. Coat Technol.* **2019**, *372*, 399–409. [CrossRef]
15. León, M.; Alvarez, D.; Valarezo, A.; Bejarano, L.; Viteri, D.; Giraldo-Betancur, A.L.; Muñoz-Saldaña, J.; Alvarez-Barreto, J. Electrodeposition of Chitosan on Ti-6Al-4V Surfaces: A Study of Process Parameters. *Mater. Res.* **2022**, *25*, e20210552. [CrossRef]
16. Sharma, A. Hydroxyapatite Coating Techniques for Titanium Dental Implants—An Overview. *Qeios* **2023**. [CrossRef]
17. Huang, C.-H.; Yoshimura, M. Biocompatible Hydroxyapatite Ceramic Coating on Titanium Alloys by Electrochemical Methods via Growing Integration Layers [GIL] Strategy: A Review. *Ceram Int.* **2023**, *in press*. [CrossRef]
18. Schwartz, A.; Kossenko, A.; Zinigrad, M.; Gofer, Y.; Borodianskiy, K.; Sobolev, A. Hydroxyapatite Coating on Ti-6Al-7Nb Alloy by Plasma Electrolytic Oxidation in Salt-Based Electrolyte. *Materials* **2022**, *15*, 7374. [CrossRef]
19. Kurup, A.; Dhatrak, P.; Khasnis, N. Surface Modification Techniques of Titanium and Titanium Alloys for Biomedical Dental Applications: A Review. *Mater. Today Proc.* **2021**, *39*, 84–90. [CrossRef]
20. Shenhar, A.; Gotman, I.; Radin, S.; Ducheyne, P.; Gutmanas, E.Y. Titanium Nitride Coatings on Surgical Titanium Alloys Produced by a Powder Immersion Reaction Assisted Coating Method: Residual Stresses and Fretting Behavior. *Surf. Coat. Technol.* **2000**, *126*, 210–218. [CrossRef]
21. Gabor, R.; Cvrček, L.; Doubková, M.; Nehasil, V.; Hlinka, J.; Unucka, P.; Buřil, M.; Podepřelová, A.; Seidlerová, J.; Bačáková, L. Hybrid Coatings for Orthopaedic Implants Formed by Physical Vapour Deposition and Microarc Oxidation. *Mater. Des.* **2022**, *219*, 110811. [CrossRef]

22. Pesode, P.; Barve, S. Surface Modification of Titanium and Titanium Alloy by Plasma Electrolytic Oxidation Process for Biomedical Applications: A Review. *Mater. Today Proc.* **2021**, *46*, 594–602. [CrossRef]
23. Darband, G.B.; Aliofkhazraei, M. Electrochemical Phosphate Conversion Coatings: A Review. *Surf. Rev. Lett.* **2017**, *24*, 1730003. [CrossRef]
24. Burduhos-Nergis, D.P.; Vizureanu, P.; Sandu, A.V.; Bejinariu, C. Evaluation of the Corrosion Resistance of Phosphate Coatings Deposited on the Surface of the Carbon Steel Used for Carabiners Manufacturing. *Appl. Sci.* **2020**, *10*, 2753. [CrossRef]
25. Burduhos-Nergis, D.-P.; Vizureanu, P.; Sandu, A.V.; Bejinariu, C. Phosphate Surface Treatment for Improving the Corrosion Resistance of the C45 Carbon Steel Used in Carabiners Manufacturing. *Materials* **2020**, *13*, 3410. [CrossRef]
26. Zhao, D.W.; Liu, C.; Zuo, K.Q.; Su, P.; Li, L.B.; Xiao, G.Y.; Cheng, L. Strontium-Zinc Phosphate Chemical Conversion Coating Improves the Osseointegration of Titanium Implants by Regulating Macrophage Polarization. *Chem. Eng. J.* **2021**, *408*, 127362. [CrossRef]
27. Zhao, D.W.; Zuo, K.Q.; Wang, K.; Sun, Z.Y.; Lu, Y.P.; Cheng, L.; Xiao, G.Y.; Liu, C. Interleukin-4 Assisted Calcium-Strontium-Zinc-Phosphate Coating Induces Controllable Macrophage Polarization and Promotes Osseointegration on Titanium Implant. *Mater. Sci. Eng. C Mater. Biol. Appl.* **2021**, *118*, 111512. [CrossRef]
28. Liu, B.; Xiao, G.; Lu, Y. Effect of PH on the Phase Composition and Corrosion Characteristics of Calcium Zinc Phosphate Conversion Coatings on Titanium. *J. Electrochem. Soc.* **2016**, *163*, C477–C485. [CrossRef]
29. Liu, B.; Xiao, G.Y.; Chen, C.Z.; Lu, Y.P.; Geng, X.W. Hopeite and Scholzite Coatings Formation on Titanium via Wet-Chemical Conversion with Controlled Temperature. *Surf. Coat. Technol.* **2020**, *384*, 125330. [CrossRef]
30. Zhao, X.C.; Dong, S.F.; Ge, B.; Huang, B.X.; Ma, J.; Chen, H.; Hao, X.H.; Wang, C.Z. Effects of Temperature and Voltage on Formation of Electrolysis Induced Chemical Conversion Coating on Titanium Surface. *Surf. Coat. Technol.* **2018**, *354*, 330–341. [CrossRef]
31. Liu, B.; Shi, X.M.; Xiao, G.Y.; Lu, Y.P. In-Situ Preparation of Scholzite Conversion Coatings on Titanium and Ti-6Al-4V for Biomedical Applications. *Colloids Surf. B Biointerfaces* **2017**, *153*, 291–299. [CrossRef] [PubMed]
32. Burduhos-Nergis, D.P.; Bejinariu, C.; Sandu, A.V. *Phosphate Coatings Suitable for Personal Protective Equipment*; Materials Research Forum LLC: Millersville, PA, USA, 2021; Volume 89, ISBN 9781644901113.
33. Axinte, M.; Vizureanu, P.; Cimpoesu, N.; Nejneru, C.; Burduhos-Nergis, D.P.; Epure, E.L. Analysis of Physicochemical Properties of W1.8507 Steel Parts with Sharp Edges, Thermochemically Treated by Plasma Nitriding with and without Polarized Screens. *Coatings* **2023**, *13*, 177. [CrossRef]
34. Owens, D.K.; Wendt, R.C. Estimation of the Surface Free Energy of Polymers. *J. Appl. Polym. Sci.* **1969**, *13*, 1741–1747. [CrossRef]
35. Xiao, G.Y.; Zhao, X.C.; Zhang, X.; Xu, W.H.; Lu, Y.P. Electric Field Induced Rapid Formation of Novel Structural Hopeite Coating on Titanium. *Mater. Lett.* **2015**, *144*, 30–32. [CrossRef]
36. Li, J.; Li, J.; He, N.; Fu, Q.; Feng, M.; Li, Q.; Wang, Q.; Liu, X.; Xiao, S.; Jin, W.; et al. In Situ Growth of Ca-Zn-P Coatings on the Zn-Pretreated WE43 Mg Alloy to Mitigate Corrosion and Enhance Cytocompatibility. *Colloids Surf. B Biointerfaces* **2022**, *218*, 112798. [CrossRef]
37. Zhao, X.C.; Xiao, G.Y.; Zhang, X.; Wang, H.Y.; Lu, Y.P. Ultrasonic Induced Rapid Formation and Crystal Refinement of Chemical Conversed Hopeite Coating on Titanium. *J. Phys. Chem. C* **2014**, *118*, 1910–1918. [CrossRef]
38. Alleborn, N.; Raszillier, H. Spreading and Sorption of a Droplet on a Porous Substrate. *Chem. Eng. Sci.* **2004**, *59*, 2071–2088. [CrossRef]
39. Trisnanto, S.R.; Setiawan, I.; Sunnardianto, G.K.; Triawan, F. Stearic Acid-Modified CuO Coating Metal Surface with Superhydrophobicity and Anti-Corrosion Properties. *J. Eng. Res.* **2019**, *2019*, 63–75.
40. Annamalai, M.; Gopinadhan, K.; Han, S.A.; Saha, S.; Park, H.J.; Cho, E.B.; Kumar, B.; Patra, A.; Kim, S.W.; Venkatesan, T. Surface Energy and Wettability of van Der Waals Structures. *Nanoscale* **2016**, *8*, 5764–5770. [CrossRef]